HIGH PRECISION CHARACTERISATION OF SEMICONDUCTOR BOLOMETERS

A. L. Woodcraft[1], R. V. Sudiwala[1], M. J. Griffin[1], E. Wakui[2], B. Maffei[1], C. E. Tucker[1], C. V. Haynes[1], F. Gannaway[1], P. A. R. Ade[1], J. J. Bock[3], A. D. Turner[3], S. Sethuraman[3] and J. W. Beeman[4]

[1]Department of Physics and Astronomy, University of Wales, Cardiff,
5, The Parade, Cardiff, CF24 3YB, UK
[2]Department of Physics, Queen Mary and Westfield College,
Mile End Road, London, E1 4NS, UK
[3]Jet Propulsion Laboratory, California Institute of Technology,
Pasadena, CA 91109, USA
[4]Lawrence Berkeley National Laboratory
Berkeley, CA 94720, USA

Abstract: We describe techniques for testing and characterising semiconductor bolometers, using the bolometer model presented in Sudiwala et. al. [1]. The procedures are illustrated with results from a prototype bolometer for the high frequency instrument (HFI) in the Planck Surveyor cosmic microwave background mission. This is a bolometer using spider-web geometry and a neutron transmutation doped (NTD) germanium thermistor, designed for operation at 100 mK. Details are given of the laboratory facility used to take data at temperatures from 70 mK to 350 mK. This employs an adiabatic demagnetisation refrigerator to cool the detector and optics. The spatial and spectral properties of the optical system are controlled using feedhorns and edge filters. To characterise the bolometer, blanked and optically loaded load curves were measured over a range of temperatures, and the response to modulated radiation was measured as a function of modulation frequency, temperature and bias current. Results for the prototype bolometer show that its behaviour is well represented by an ideal thermal detector down to a temperature of approximately 100 mK. Below this, non-thermal effects such as electron-phonon decoupling or electric field dependent resistance appear to lead to departure from ideal behaviour. The performance was in good agreement with the design goals for the bolometer.

]**International Journal of Infrared and Millimeter Waves, 23(4):575-595, 2002**

1 Introduction

Today, bolometers are the best choice for direct detection of radiation at wavelengths between 200 μm and 3 mm (e.g. references [2, 3]), and can be competitive for wavelengths between 100 μm and 2 mm. Currently, state-of-the-art detectors consist of a germanium semiconductor thermistor bonded to a metallised silicon nitride absorber, cooled to temperatures between 100 and 300 mK [4]. Neutron transmutation doped (NTD) germanium [5, 6] is normally used, since other doping methods cannot provide

a sufficiently uniform level of doping. Ideal bolometer theory [1, 2, 7] can be used to accurately characterise the noise and thermal properties of NTD bolometers.

Optimising a bolometer requires a good understanding and control of the key parameters: the temperature dependence of the thermistor resistance, the heat capacity of the thermistor and absorber, and the thermal conductance between the absorber and the heat sink. A detailed theory for modelling such parameters is presented in reference [1], hereinafter Paper I. In this paper we discuss the experimental details of making the measurements required to use such a model.

These methods are illustrated with results from tests on a prototype 100 mK bolometer for HFI; the high frequency instrument [8] in the Planck Surveyor cosmic microwave background imaging satellite [9]. This mission aims to measure anisotropies in the cosmic microwave background radiation over the whole sky, to a sensitivity of a few parts per million. This requires the most sensitive bolometers available, with very good control of the spatial response of the feed optics, since strong sources such as the sun and the earth are much brighter than the anisotropies to be measured. The design goals of the bolometer are, at 100 mK, a static thermal conductance of 110 pWK^{-1}, a heat capacity of 0.2 pJ K^{-1}, a time constant below 5.8 ms, and an electrical NEP of 1.5×10^{-17} WHz$^{-0.5}$ or better. We present results for the thermal parameters and responsivity of the prototype detector. Noise measurements on similar devices have shown that NTD spider-web bolometers exhibit negligible excess noise down to frequencies as low as 100 mHz [10].

The structure of the paper is as follows. In section 2, we describe our bolometer test facility; in section 3, details of the bolometer and optical system used for the measurements described here are given. Section 4 describes characterisation of bolometers in general, illustrated by measurements of the system described in section 3.

2 Bolometer test facility

2.1 Requirements

From the thermal model presented in Paper I, it can be seen that there are various requirements for a bolometer characterisation facility.

The basic measurement is the bolometer voltage as a function of bias current (load curve). To allow accurate derivation of the main bolometer parameters, the facility must allow load curves to be made over a range of currents, with the bolometer heat sink held at a range of accurately measured temperatures down to at least the intended operating temperature.

Good control is required over the optical power incident on the bolometer. “Blanked” measurements are required with this power effectively zero. In practise, this means that the effect of absorbed power on the bolometer temperature must be negligible.

Measurements are also required with the bolometer exposed to a well defined optical power over a well defined spectral band. This power should be representative of the expected background power on the bolometer in use, and it should be possible to modulate it on a timescale faster than the bolometer speed of response.

2.2 The facility

The results presented here were all obtained using an adiabatic demagnetisation refrigerator (ADR). This enables temperatures below 100 mK to be achieved, and is well suited for detector characterisation since it allows rapid and controlled temperature changes.

The cryostat, shown in Figure 1, contains an 11 litre nitrogen bath used to reduce boil-off from the helium bath, as well as to maintain filters at approximately 77 K. The helium bath has a capacity of 6 litres, and can be cooled to a temperature of approximately 1.6 K by pumping on the vapour above the helium bath using a rotary pump. Further cooling is provided by a chromium potassium alum (CPA) demagnetisation stage (hereinafter referred to as the 'stage') in the bore of a 6 T superconducting magnet[1]. This provides cooling and temperature adjustment to temperatures below 70 mK. The stage temperature is not automatically regulated, but drifts upwards at a rate of up to approximately 70 μK/minute. The stage and salt pill are supported using Kevlar cords in tension [11], to minimise the thermal conduction to the helium bath. The magnetic field at the bolometer is compensated so that in normal operation the bolometer experiences a field which we estimate to be less than 3 mT. The hold time at 100 mK is approximately 12 hours, the limiting factor being the capacity of the pumped helium bath.

A mechanical heat switch is used to make and break thermal contact between the helium bath and the salt pill. To make contact, a solenoid is used to press a tongue protruding from the salt pill support between a moveable plunger and an anvil. All components in thermal contact are made from gold-plated copper. The solenoid is an off-the-shelf item, with the magnet replaced with a samarium cobalt magnet. It latches in both the open and closed position, with current only being required during opening or closing.

Temperatures in the cryostat are monitored with two types of thermometer. The temperature of the stage is measured using a neutron transmutation doped (NTD) germanium (Haller-Beeman type #12 [6]) thermometer, read out using an AVS-47 cryogenic resistance bridge[2]. This thermometer has been calibrated against germanium secondary standard thermometers based on the ITS-90 temperature scale[3]. Temperatures at other points in the cryostat are determined using BCY71 transistors. Measurement of the forward voltage drop across the base-collector junction provides useful thermometry for temperatures from 1 K up to room temperature.

The bolometer is mounted on the stage, which during characterisation is usually maintained at a temperature between 70 and 350 mK. An important consideration in the construction of the cryostat is the protection of the bolometer from unwanted radiation. This comes mainly from two sources: blackbody radiation from components within the dewar that are warmer than the detector, and straylight reaching the detector from outside the cryostat. For 'blanked' tests, the stage is surrounded by a

[1] American Magnetics Inc, Oak Ridge, Tenessee
[2] RV-Elektroniikka Oy, Vantaa, Finland
[3] Lake Shore Cryotronics Inc, Westerville, Ohio, model GR-200A-30

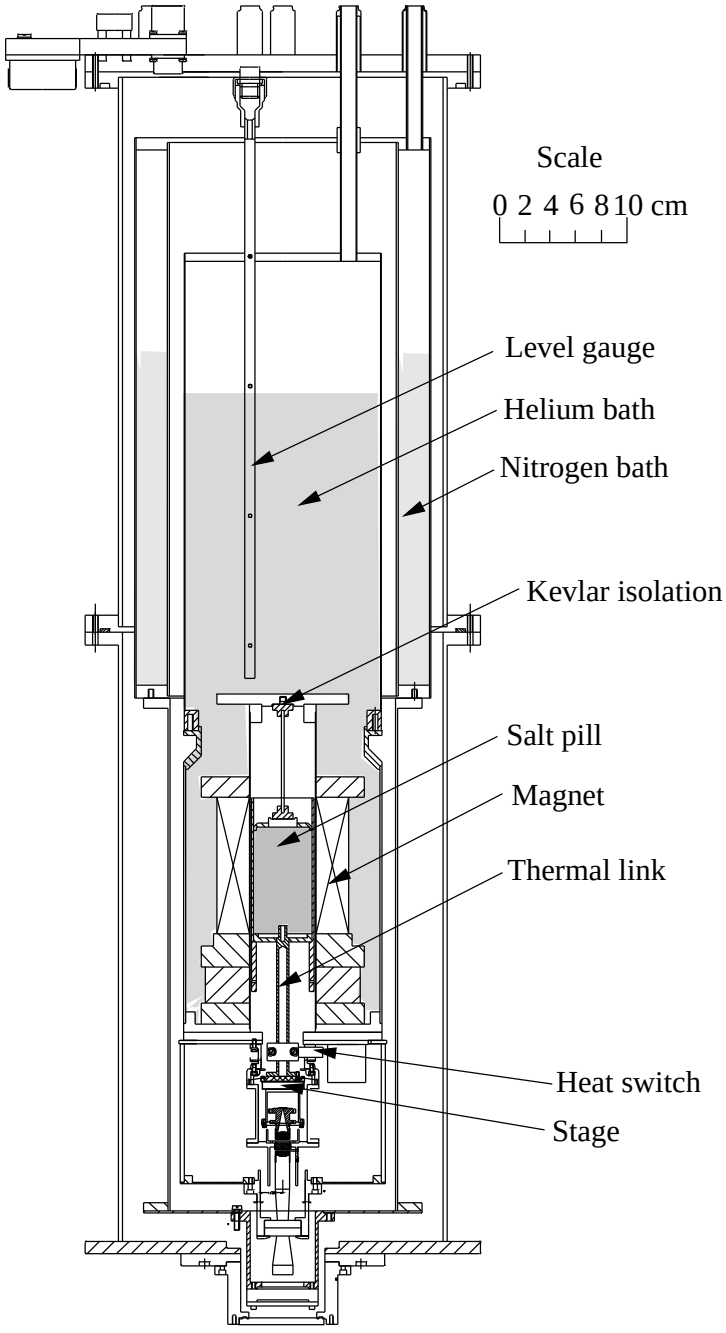

Figure 1: The test facility adiabatic demagnetisation cryostat, configured for the measurements described here.

radiation shield maintained at the helium bath temperature. Careful attention is paid to the integrity of this shield, especially around wiring feedthroughs. There are additional shields at helium and nitrogen bath temperatures, both wrapped with multilayer superinsulation. These shields are also protected against the entry of light, as is the outer shell of the cryostat at room temperature.

Metal surfaces in the cryostat at helium bath temperature and below are gold plated to provide good thermal contact and low emissivity.

2.3 Optical design

For tests in which the bolometer is exposed to a radiation source outside the cryostat, an optical path is opened up through the radiation shields. Radiation enters the dewar through a rigid polyethylene window, which has a transmittance of approximately 90% over the wavelength range used.

Low (frequency) pass optical filters are used on all the radiation shields. These provide rejection of blackbody radiation from higher temperatures, reducing the thermal load on the helium bath and stage, as well as controlling the wavelengths reaching the bolometer. Most of the blackbody radiation reaching lower temperatures from room temperature is absorbed by the nitrogen bath, which has a much larger cooling capacity than the helium bath and the demagnetisation stage.

With the exception of a Fluorogold filter on the 77 K shield, reflective metal mesh capacitative grid filters are used for the low pass elements [12]. These add less blackbody radiation to the beam than absorption filters. Not only do they have lower emissivity, but they remain at lower temperatures since most of the unwanted radiation is reflected (rather than being absorbed), and their thermal conductance is relatively high. They also have the advantages of a sharp cut-off, high pass-band transmission, and high stop-band rejection.

In addition, a neutral density filter is used to reduce the detector power loading from an external source to the required level. The temperatures of the filters on the helium and nitrogen bath shields are monitored by thermometers mounted on the shield at the edge of the filter. Knowledge of these temperatures is important since the blackbody radiation from these filters can be a significant component of the overall power incident on the bolometer.

2.4 Electrical configuration

The electrical configuration used for the bolometer bias and readout is shown in Figure 2. A bias voltage is applied to two 60 MΩ load resistors in series with the bolometer, providing an approximately constant current at a given bias voltage. To minimise Johnson noise from the load resistors, they are mounted on the stage. The voltage across the bolometer is measured by a matched pair of IFN146 silicon JFET source followers, coupled to a low noise external amplifier. To reduce sensitivity to microphonics and pick-up, a differential configuration is used. In addition, the wiring length from the detectors is made as short as possible by mounting the JFETs on the helium

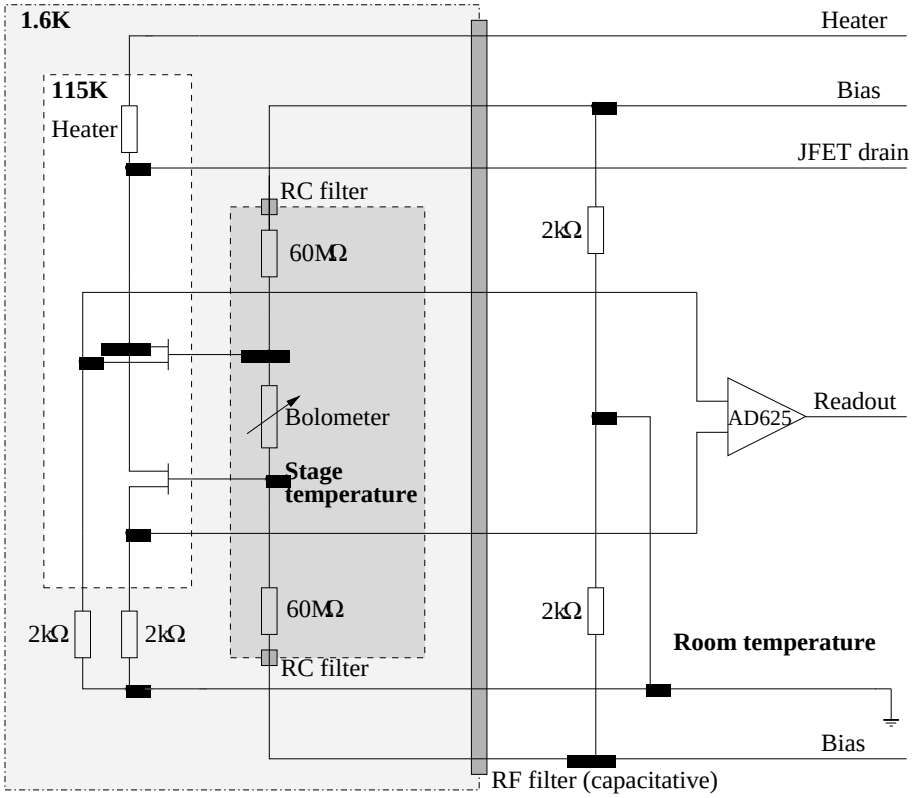

Figure 2: The bolometer bias and readout system. The shading shows regions maintained at different temperatures

bath. The JFETs have a noise minimum at a temperature of 110-120 K, and are therefore mounted on a weak thermal link, and heated to the required temperature by a metal film resistor. A light-tight shield prevents thermal radiation from this temperature from contaminating the inside of the 1.6 K shield.

All signal lines entering the cryostat include capacitative filters to reduce electromagnetic interference. Further RC filtering is used on the bias lines where they enter the 100 mK enclosure. The readout lines are not filtered at this point, since this can significantly alter the electrical time constant, and thus the measured speed of response of the bolometer. To reduce the effect of microphonics, wiring in the dewar is formed of twisted pairs, held in place with GE 7031 varnish.

3 Bolometer and feed optics design

The measurements described in this paper were carried out on a prototype 143 GHz bolometer for Planck HFI. The optical system, shown in Figure 3, was set up to resemble the planned layout for HFI, except that in HFI a corrugated feedhorn will be used at 100 mK. This scheme is described in more detail in reference [13].

Beyond the nitrogen shield filter, the optical system incorporates sections held at different temperatures, and separated by small vacuum gaps. The outer section is thermally linked to the 1.6 K stage, but incident radiation heats it to approximately 8 K. A profiled, flared, corrugated feedhorn, followed by a length of waveguide, determines the illumination pattern and the low frequency edge of the pass-band. A second corrugated feedhorn, followed by a polypropylene lens and a filter, recollimates the beam. After a small vacuum gap, it then passes through a stack of filters on the inner 1.6 K radiation shield.

After another vacuum gap, the beam passes through a second filter/lens combination, followed by a smooth-walled conical feedhorn. This concentrates the radiation onto the bolometer, which is contained within an integrating cavity in a light-tight module. These components are all thermally anchored to the stage.

The passband of radiation reaching the bolometer is defined by the waveguide section at the end of the first feedhorn and a low-pass filter in front of the final feedhorn. The system is single-moded, and the throughput should therefore be λ^2, where λ is the radiation wavelength.

Other low-pass filters at stage temperature, 1.6 K and 8 K block radiation which would otherwise be admitted through harmonic leaks [12], and reduce the amount of thermal radiation penetrating to lower temperatures. A germanium coated mylar 0.9% neutral density filter at 1.6 K reduces the radiation from a room temperature external load to approximately the design value for the bolometer. The filtering scheme is shown in Table I, while measured transmission profiles for the filters from the helium bath inwards are shown in Figure 4.

The bolometer is a composite "spider-web" device [4], contained in an integrating cavity within a light-tight module. The absorber consists of a 3.4 mm diameter free-standing gold metallised silicon nitride mesh with 425 μm grid spacing. The temperature sensor is a $25 \times 300 \times 100$ μm NTD germanium (Haller-Beeman #19 [2]) chip, indium bump bonded to the centre of the mesh. Electrical contact to the thermistor is made by extending the metallisation along two of the absorber supports. These leads also dominate the thermal conductance to the absorber.

4 Characterisation of bolometers

4.1 Blanked load curves

To characterise a bolometer, various sets of measurements are carried out. First, the bolometer is measured in the "blanked" configuration, so that it is exposed to negligible external radiation. Load curves are obtained at a range of stage temperatures,

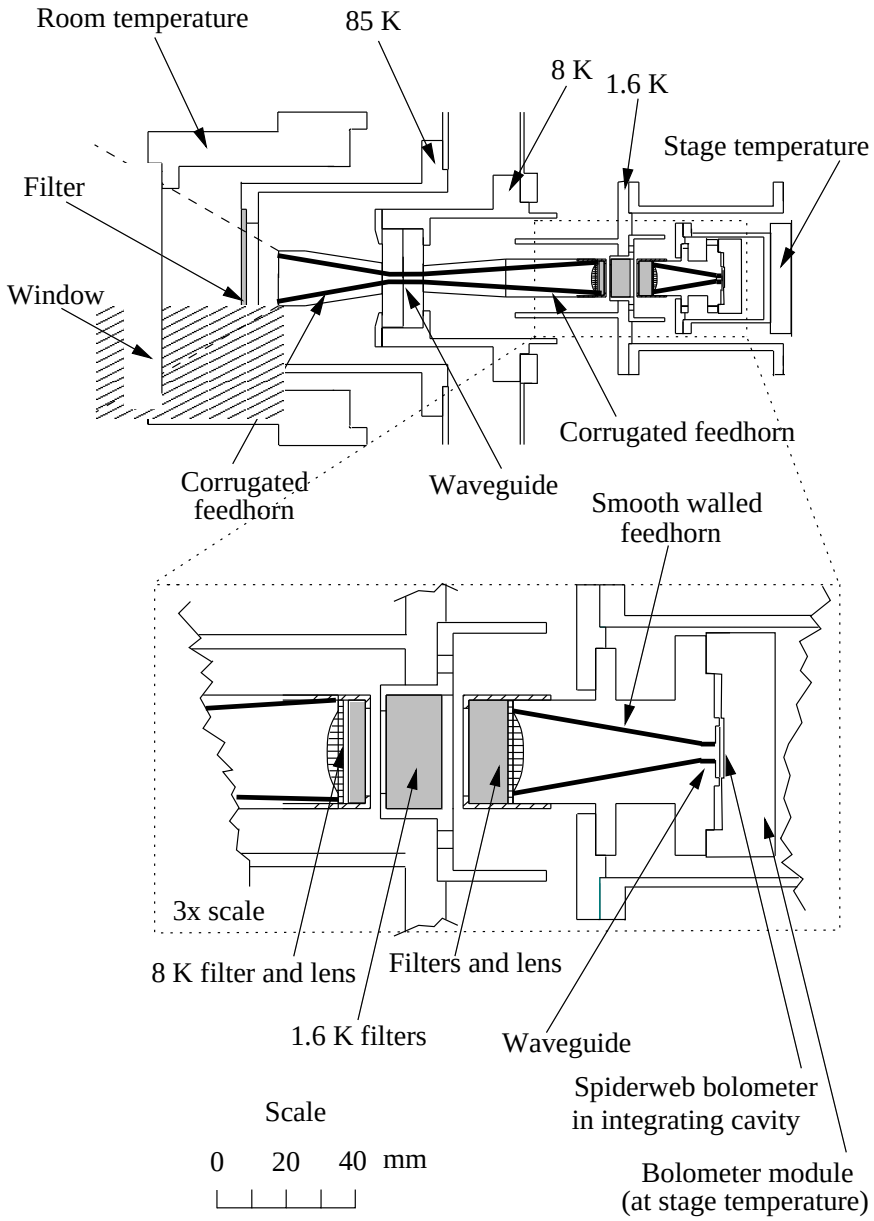

Figure 3: The optical layout. More details on the filtering scheme are given in Table I.

Temperature	Filter	Transmission
300 K	polyethylene	0.90
85 K	1.2 mm thick Fluorogold filter	0.97
8 K	polypropylene lens	0.90
	Feedhorns: 4.3 cm^{-1} cut-off	0.90
	7.5 cm^{-1} low-pass filter	0.91
1.6 K	14 cm^{-1} low-pass filter	0.92
	18 cm^{-1} low-pass filter	0.89
	Neutral density filter	0.009
100 mK	5.8 cm^{-1} low-pass filter	0.65
	43 cm^{-1} low-pass filter	0.92
	polypropylene lens	0.90
	Feedhorn: 4.1 cm^{-1} cut-off	0.50

Table I: The filtering scheme. Measured transmission values are used for the filters; values for other components are estimates.

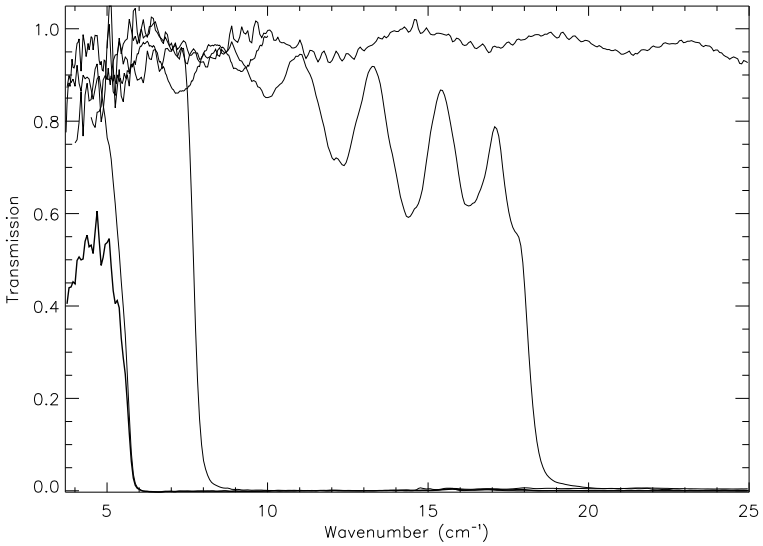

Figure 4: Measured transmission profiles for the edge filters at helium bath temperature and below (thin lines), along with the total transmission obtained by multiplying each profile (thick line). (Note that the 14 cm^{-1} filter was only measured up to 10 cm^{-1}).

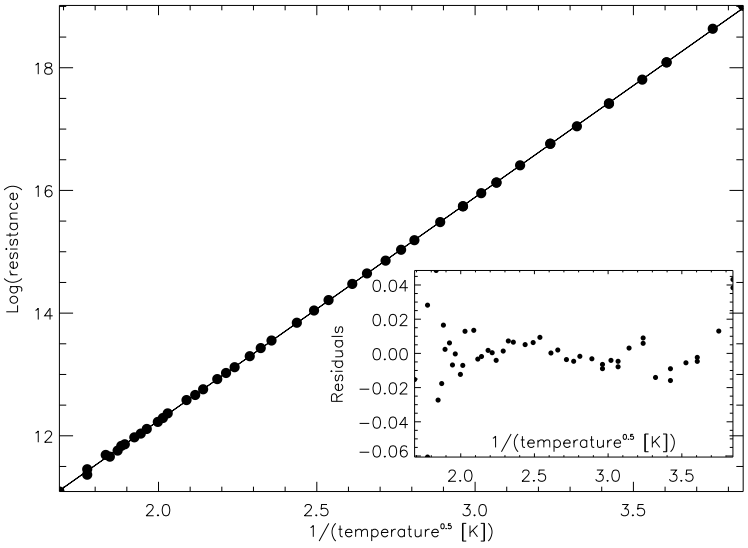

Figure 5: Zero bias resistance - temperature relationship for the bolometer thermistor from blanked measurements (filled circles) along with a linear fit (straight line). The insert shows the fit residuals.

in this example from 70 to 350 mK, by stepping the bias current through the device, and measuring the resulting voltage across it. The zero bias resistance, R_0, at each temperature (i.e. the resistance in the absence of self-heating) is then determined by extrapolation of the low-current portions of the load curves. This enables the resistance vs temperature characteristics of the thermometer element in the bolometer to be calculated.

The thermistor resistance, R, is expected to vary with temperature, T, as (Paper I)

$$R = R^* \exp\left(\frac{T_g}{T}\right)^n, \tag{1}$$

where R^* and T_g are constants depending on the thermistor doping and, for R^*, on its dimensions. The coefficient n is usually taken to be 0.5. Our measurements are found to correspond extremely well to this relationship, with $n = 0.5$ - see Figure 5. The lack of significant systematic behaviour in the fit residuals shows that the choice of n produces a good fit[4]. This also shows that, as intended, the absorbed optical power is negligible (Paper I). We find values of $T_g = 13.3 \pm 0.1$ K and $R^* = 143 \pm 4\ \Omega$. The value of T_g should depend only on the type of material; for the same type, other groups have found values of 21.2 K [15], 16.0 K [16] and 14.7 K [17].

[4]This does not appear to always be the case for NTD germanium [14]

Once these parameters have been determined, the thermal model described in Paper I is used to fit each load curve. The two free parameters in the model, G_{S0} and β, describe the conductance of the thermal link between the bolometer absorber and the stage, with G_{S0} representing the (static) thermal conductance at the stage temperature, T_0, and β giving the power-law coefficient for the temperature variation of G_{S0} over the range of *absorber* temperatures involved (Paper I). The incident power, Q, is set to zero.

For each load curve taken at stage temperature T_0, the parameters $\beta(T_0)$ and $G_{S0}(T_0)$ are determined. As can be seen from Figure 6, apart from small departures below 100 mK, the thermal model produces excellent fits to our measurements for the complete family of load curves, using the same values for R^* and T_g for all temperatures. Moreover, the derived values of β and G_{S0} are self-consistent across the whole set of load curves. For an ideal bolometer (i.e. one which obeys the assumptions made in deriving the bolometer model), each load curve will have the same value of β, while G_{S0} can be calculated[5] for any stage temperature given the value at some temperature T_0':

$$G_{S0}(T_0) = G_{S0}(T_0') \left(\frac{T_0}{T_0'} \right)^{\beta}. \tag{2}$$

Figure 7 shows β as a function of stage temperature. It can be seen that the values of β above 150 mK are approximately constant. The value of β can also be obtained from the temperature variation of $G_{S0}(T_0)$, using equation 2. This is shown in Figure 8. Note the excellent agreement between the blanked and unblanked data - the system was thermally cycled between these sets of data. The figure includes a power law fit to the conductance data above 150 mK. The resulting coefficient $\beta = 0.99 \pm 0.01$ is in good agreement with the individual values for β shown in Figure 7; the different load curves are thus self-consistent. Since the conductance is expected to be dominated by the metallised leads, a value close to $\beta = 1$, due to electronic thermal conductivity, is expected [18].

Below 150 mK, the temperature variation of the conductance becomes larger, as seen both by the 10% increase in β below 150 mK in Figure 7 and the increase in slope below 150 mK in Figure 8. In fact, at these temperatures, the derived value of β for a given *stage* temperature depends on the range of *bolometer* temperatures used for fitting. This suggests that the ideal bolometer model has broken down, and the conductivity cannot be represented by a single power-law. A likely cause is an additional thermal impedance due to electron-phonon decoupling within the thermistor [19, 20], although electric field effects [20] could produce similar effects.

However, above 100 mK, the change in β is at worst around 10%, and the entire dataset can still be represented well by just four parameters: T_g, R^*, β and, for some temperature T_0', $G_{S0}(T_0')$. Taking β and $G_{S0}(T_0')$ from the fit to Figure 8 and applying the thermal model produces a family of load curves which agree with the data to

[5] It should be noted that this expression is only true for the (static) conductance when the bolometer is at the stage temperature (G_{S0}). It does not give the conductance at an arbitrary bolometer temperature (G_S), since it does not allow for the variation of conductivity with temperature across the thermal link (Paper I).

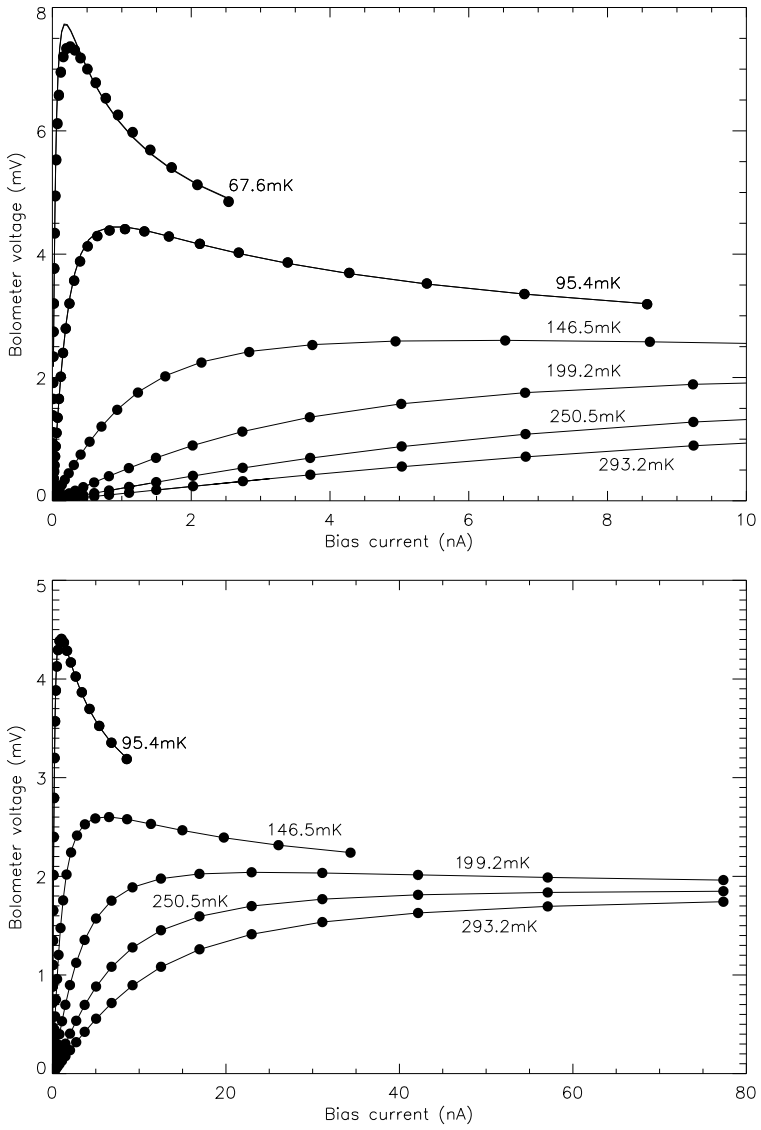

Figure 6: Thermal model fits (lines) to blanked data (filled circles) for a subset of stage temperatures. The two graphs show the same data over different bias current ranges.

better than 2%, except at extremely low biases. It is therefore possible to predict the behaviour of the bolometer accurately for temperatures at which it was not measured.

The conductance value obtained is G_{S0}(100 mK)=150 pWK^{-1}. Additional measurements on a nominally identical bolometer gave similar results to the first bolome-

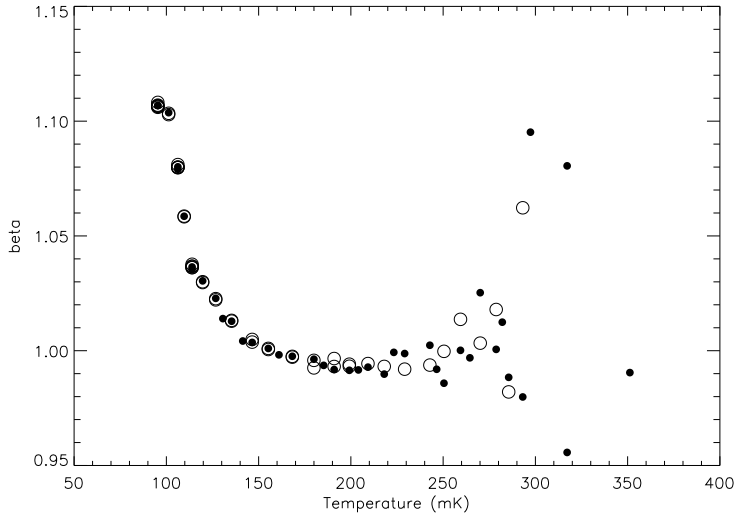

Figure 7: Value of the power law coefficient of the temperature dependence of the thermal conductance, β, as a function of stage temperature, derived from thermal model fits to individual load curves. Filled (open) circles represent blanked (unblanked) data.

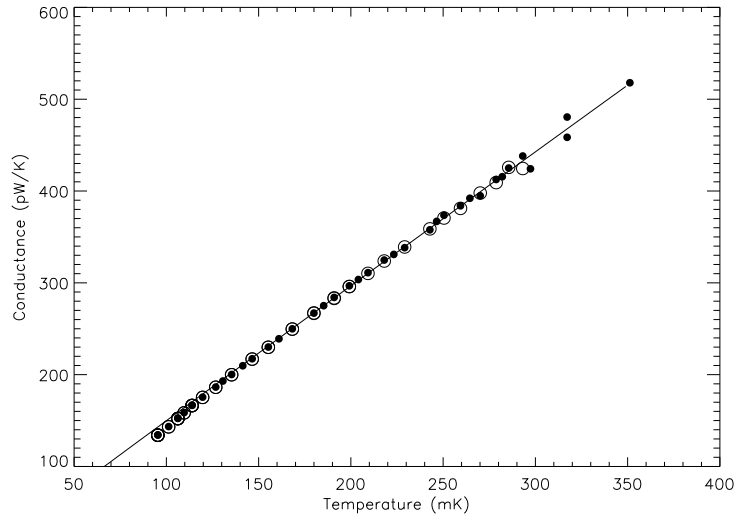

Figure 8: Value of the static thermal conductance, G_{S0}, at each stage temperature, derived from fits to individual load curves. Filled (open) circles represent blanked (unblanked) data. The line is a power-law fit to the data above 150 mK.

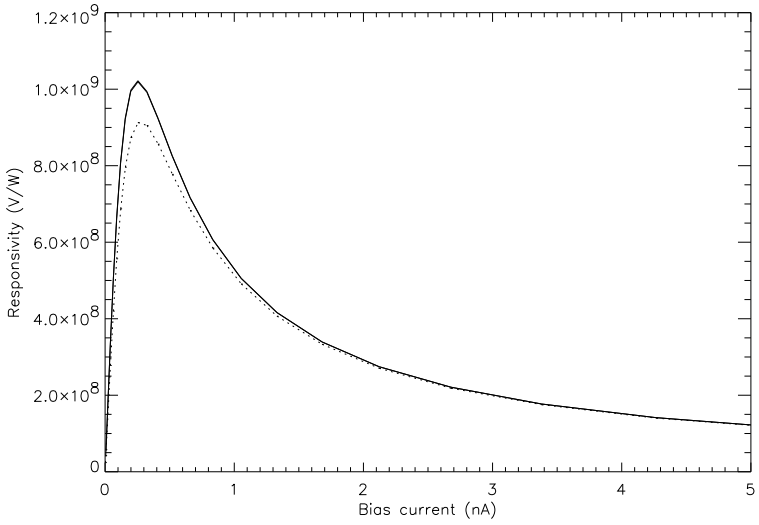

Figure 9: Small-signal optical responsivity at 100 mK predicted from the thermal model, with the bolometer blanked (solid lines) and exposed to a 300 K load (dashed lines)

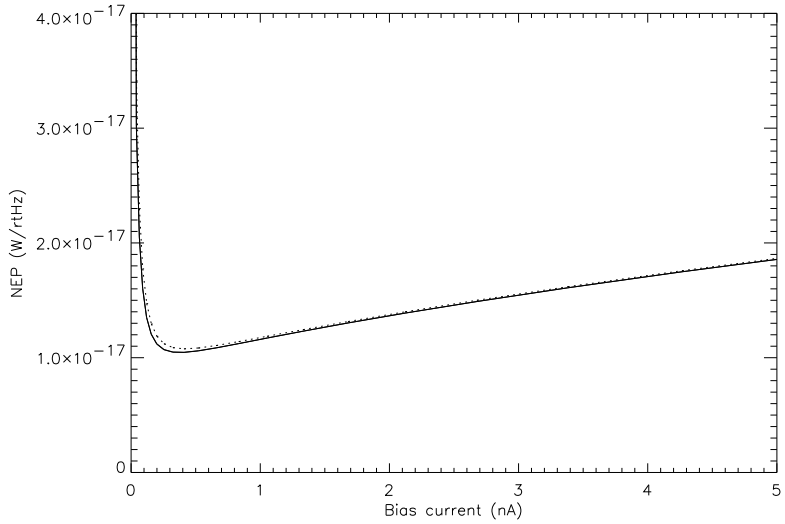

Figure 10: Ideal (Johnson + phonon noise) NEP at 100 mK predicted from the thermal model, with the bolometer blanked (solid lines) and exposed to a 300 K load (dashed lines)

ter, with values of β=1.18 and G_{S0}(100 mK)=132 pWK^{-1}. These values of G_{S0} are both close to the design value of 110 pWK^{-1}.

The thermal model can also be used to predict the optical responsivity (dV/dQ, for change in voltage V as a response to a change in power Q), and NEP (Paper I) for the bolometer in the blanked configuration. These are shown, for the planned operating temperature of 100 mK, in Figures 9 and 10. It can be seen that the goal of an NEP under 1.5×10^{-17} WHz$^{-0.5}$ is easily met.

4.2 Static optical load tests

After characterisation in the blanked configuration, the bolometer is then opened to radiation from outside the cryostat. Our optical load consists of Eccosorb AN72[6] either at room temperature or soaked in liquid nitrogen, placed so that it fills the beam. Load curves are taken at the same temperatures as before, allowing straightforward comparison with data from the blanked configuration. The thermal model is then applied again, this time allowing the loading parameter Q to vary. For our measurements, values for β and G_{S0} almost identical to those from the blanked measurements were found (see Figures 7 & 8). It should be noted that the derived values of β and G_{S0} do not depend on the value used for the stage temperature (except that G_{S0} is defined with respect to the chosen value). If an incorrect stage temperature is used, a different (incorrect) value for the absorbed power, Q, will be produced, but the values of β and G_{S0} will be unchanged (Paper I).

Figure 11 shows the derived values for the absorbed power under a room temperature load, with a mean value of 0.34 pW (taken from measurements below 200 mK, where the scatter is small). This value should not depend on the bolometer temperature, although as the temperature increases and the bolometer becomes less sensitive, the measurement errors become larger.

It is also possible to derive the absorbed power directly from the zero-bias bolometer temperature (Paper I). Such values are also shown in Figure 11. As would be expected, both methods produce similar results.

The optical efficiency of the system can be calculated by comparing the absorbed power with a predicted value for the incident power. In order to cancel out any excess power on the bolometer, the difference in power between a pair of load curves under different (room temperature and liquid nitrogen) optical loads is used. For a bolometer which can be accurately described by the thermal model, this method also cancels out the effect of any error in the stage temperature, since such an error produces an effect identical to excess power (Paper I). It is thus only necessary to ensure that the stage temperature is the same for both load curves; knowledge of the absolute temperature is not required.

Excess power can come from straylight and thermal emission from components in the field of view of the bolometer within the cryostat. In particular, the filters in the beam are a source of thermal radiation. However, the filter temperature depends on

[6]Emerson and Cuming Microwave Products, Inc., 28 York Avenue, Randolph, MA 02368, USA

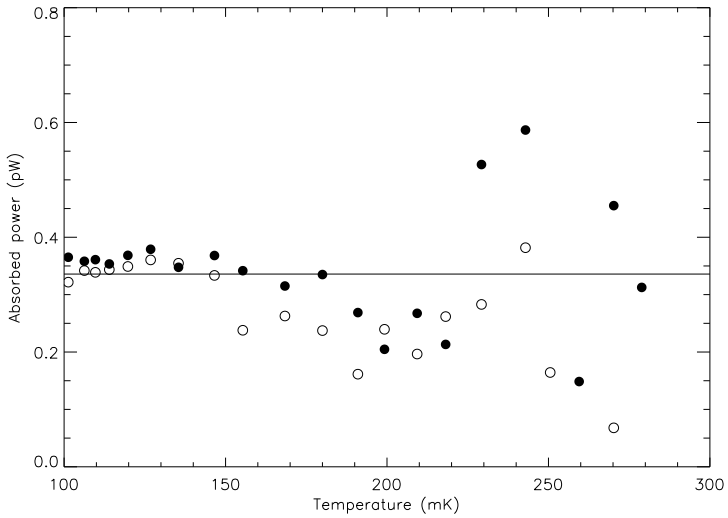

Figure 11: Absorbed power for 300 K optical load. Filled circles represent values taken by fitting absorbed power, Q, in the thermal model; unfilled circles represent values taken from the zero-bias bolometer temperature. The line shows the mean value taken from the filled circles below 200 mK

the thermal load, and the excess power is therefore load dependent. Measurements of the variation in excess power with filter temperature show that failing to take this into account would cause a systematic error of around 25% in our measurements. To minimise the problem, measurements were taken immediately before and after changing the load, so that the filters did not have time to change temperature significantly.

The power difference, ΔQ, can be determined from the absorbed power for each load curve from the thermal model fits. Alternatively, the difference in electrical power as a function of bolometer temperature (or equivalently, resistance) can be calculated directly from a pair of load curves. Since the total power at a given bolometer temperature must be the same, this difference is equal to the difference in absorbed power.

At 100 mK, the incident power difference calculated from the thermal model is 0.18 pW (compared to values of 0.16 to 0.20 pW, depending on bolometer temperature, taken directly from the load curves). Using measured values for the transmission of the filters and room temperature window (see Figure I), this gives an efficiency of 19% for the feed optics (i.e. the feedhorns and lenses) and the bolometer itself. The efficiency of the feedhorns is less well known than the filters. Using approximate values (see Table I) for the feedhorn and lens transmission gives a value of 50% for the efficiency of the bolometer itself. The use of a corrugated horn at 100 mK should significantly improve the efficiency of the feed optics [21].

Such measurements under two different optical loads can also be used to calculate

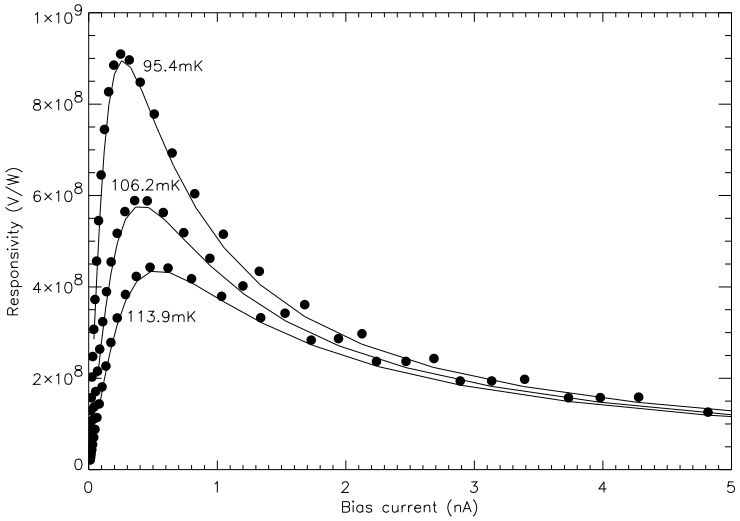

Figure 12: Large-signal optical response referred to absorbed power, from measurements with 300 K and 77 K load (filled circles), compared to the predictions of the thermal model (solid lines)

the large-signal optical response. Figure 12 shows the response with respect to absorbed power. This is obtained by calculating the voltage difference between points at the same bias current from each pair of load curves. This is then divided by the difference in absorbed power taken directly from the load curves as described above. This is not equivalent to the small scale responsivity predicted in Figure 9, because the power difference is too large. However, the thermal model fits to each pair of load curves can be used to predict the appropriate response - this is also shown in Figure 12.

4.3 Chopped optical load tests

As well as measurements with static loads, the detector response is measured using a chopper which switches the load from room temperature eccosorb to a reflective load. In our tests, for various stage temperatures and bias currents, the chopper frequency was increased from 1.5 Hz to 250 Hz, while measuring the response from the detector using a phase sensitive detector locked to the chopper frequency.

The data can be extrapolated to zero frequency to obtain the variation of DC response as a function of stage temperature and bias. These results are shown in Figure 13, and compared to the responsivity predicted from the thermal model, for a 300 K optical load. For the chopped loads, the magnitude of the modulated power is difficult to calculate. The results, in arbitrary units, have therefore all been multiplied by a common normalisation factor to provide the best agreement with the theoretical data.

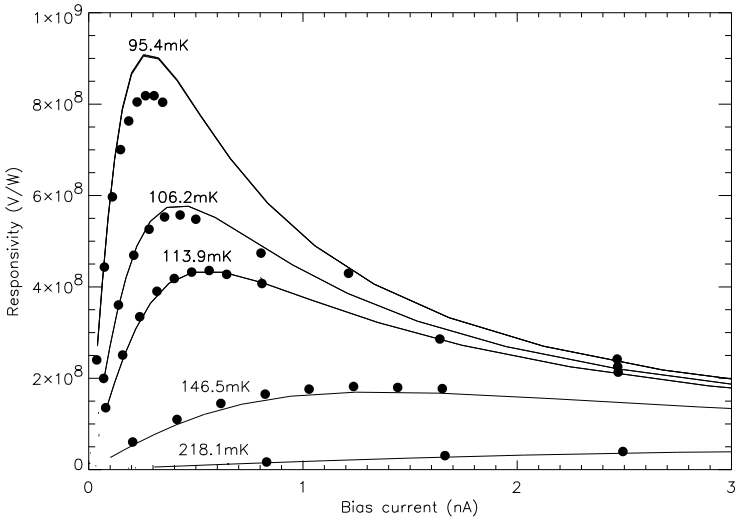

Figure 13: Optical response referred to absorbed power, from measurements using a chopped load (filled circles), compared to optical responsivity predicted from thermal model fits to load curves under a 300 K load (solid lines). The experimental data are normalised to the theoretical values (see text).

The results from the chopped load measurements are also used to calculate the detector time constant. The results of measurements at various stage temperatures and biases are shown in Figure 14. Each measurement could be well represented by a single time constant. The results are well within the design goal of a time constant under 6 ms. The consistency of this data set can be seen if the time constants are converted to heat capacity. This is obtained by multiplying the time constants by the effective thermal conductance (Paper I), and is shown in Figure 15. The thermal conductance is taken from the thermal model results, using the fit to the data in Figure 8. A power law fit to the heat capacity data gives a value of $2.9(T/1\mathrm{K})^{1.2}$ pJ K^{-1}, using data from 120 mK upwards. This corresponds to a 100 mK value of 0.21 pJ K^{-1}, compared with the design value of 0.2 pJ K^{-1}. Since the heat capacity is due to a mixture of metallic and non-metallic components, a power-law coefficient between 1 and 3 would be expected.

The data for bolometer temperatures below 120 mK do not fall onto the fit line. Again, this could be due to non-thermal effects in the bolometer.

5 Conclusions

We have described methods for testing and characterising semiconductor bolometers, using the model presented in Paper I. Results from a neutron transmutation doped

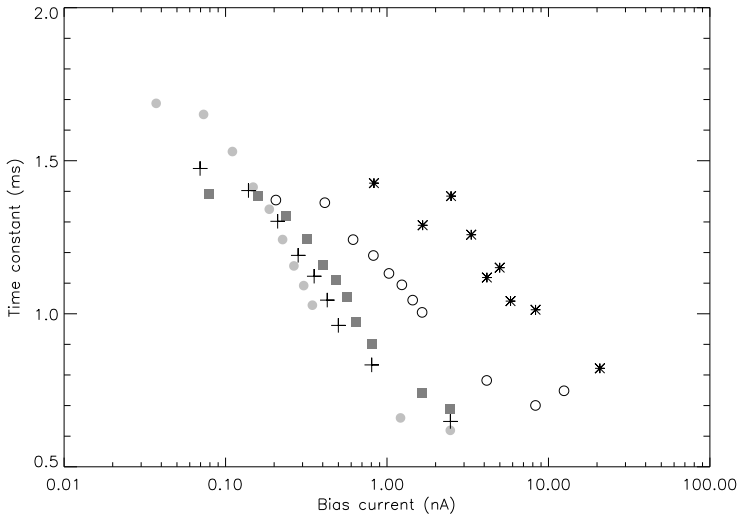

Figure 14: Bolometer time constant as a function of bias, for different stage temperatures (light grey circle: 100 mK, cross: 110 mK, grey box: 120 mK, open circle: 150 mK, star: 220 mK)

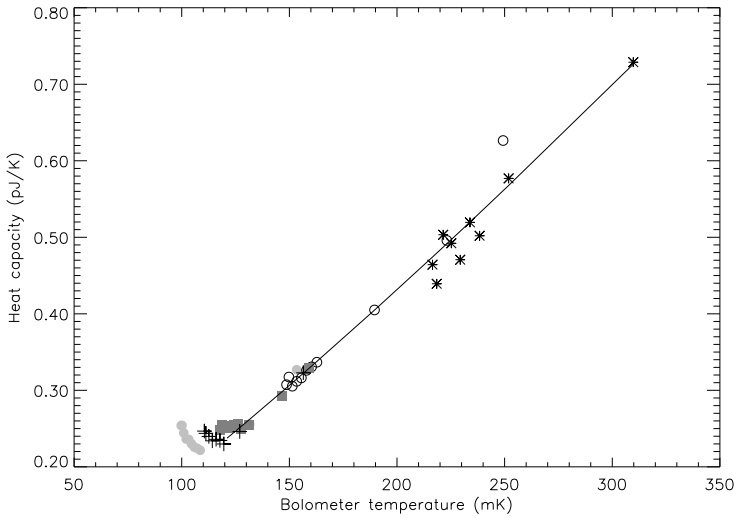

Figure 15: Bolometer heat capacity as a function of bolometer temperature, with a fit to the data at 120 mK and above. The points were obtained at the following stage temperatures: light grey circle: 100 mK, cross: 110 mK, grey box: 120 mK, open circle: 150 mK, star: 220 mK.

(NTD) germanium bolometer, a prototype for the Planck Surveyor mission, were used as illustration.

We have demonstrated that with such a bolometer, and sufficiently good experimental equipment and procedures, excellent agreement with the ideal bolometer model can be achieved over a wide range of temperatures. With such good agreement, the behaviour of a bolometer can then be predicted accurately for an arbitrary temperature and power loading using just the four free parameters in the bolometer model.

While non ideal effects appear to be significant below 100 mK, the behaviour of the Planck HFI bolometer was in excellent agreement with the bolometer model at temperatures of 100 mK and higher. The results were repeatable after thermal cycling. In addition, a second bolometer with the same design parameters showed nearly identical properties. The properties were a good match to the design goals for the bolometers.

Acknowledgements

We are grateful to the UK Particle Physics and Astronomy Research Council which has supported this work through grants for instrumentation research & development and the Planck HFI project, and through a studentship for EW.

References

[1] (Paper I) Sudiwala RV, Griffin MJ, Woodcraft AL. Thermal modelling and characterisation of semiconductor bolometers. Int. J. Infrared. Mill. Waves 2002; 23,545.

[2] Richards PL. Bolometers for infrared and millimeter waves. J. App. Phys. 1994; 76:1.

[3] Griffin MJ. Bolometers for far-infrared and submillimetre astronomy. Nuc. Instrum. Methods. Phys. Res. Sec. A 2000;444:397.

[4] Mauskopf PD, Bock JJ, Castillo HD, et al. Composite infrared bolometers with Si_3N_4 micromesh absorbers. Applied Optics 1997;36:765.

[5] Haller EE. Advanced far-infrared detectors. Infrared Phys. & Tech. 1994;35:127.

[6] Haller EE, Itoh KM, Beeman JW. Neutron transmutation doped (NTD) germanium thermistors for sub-mm bolometer applications. Proc. 30th ESLAB Symp. “Submillimetre and Far-Infrared Space Instrumentation”, 24-26 September 1996, ESA 1996;SP-388:115.

[7] Mather JC. Bolometer noise: nonequilibrium theory. Applied Optics 1982; 21:1125.

[8] Lamarre JM, Ade PAR, Benoît A, et al. The high frequency instrument of Planck: Design and performances. Astro. Lett and Communications 2000;37:161.

[9] Mandolesi N, Villa M. FIRST/Planck mission. In V Piuri, M Savino, editors, ICMT/99. Proceedings of the 16th IEEE Instrumentation and measurement technology conference, IEEE, Piscataway, NJ, USA, volume 2. 1999;975

[10] Bock JJ, DelCastillo HM, Turner AD, et al. Infrared bolometers with silicon nitride micromesh absorbers. Proc. 30th ESLAB Symp. "Submillimetre and Far-Infrared Space Instrumentation", 24-26 September 1996, ESA SP-388;119.

[11] Duband L, Hui L, Lange A. Thermal isolation of large loads at low temperature using Kevlar rope. Cryogenics 1993;33:643.

[12] Lee C, Ade PAR, Haynes CV. Self supporting filters for compact focal plane designs. Proc. 30th ESLAB Symp. "Submillimetre and Far-Infrared Space Instrumentation", 24-26 September 1996, ESA SP-388 1996;81.

[13] Maffei B, Ade PAR, Tucker CE, et al. Shaped corrugated horns for cosmic microwave background anisotropy measurements. Int. J. Infrared. Mill. Waves 2000;21:2023.

[14] Woodcraft AL, Sudiwala RV, Wakui E. Measurement of anomalous resistance-temperature relation for neutron transmutation doped germanium. In Proceedings of Low Temperature Detectors 9 (to appear). AIP 2002.

[15] Soudée J, Broszkiewicz D, Giraud-Héraud Y, et al. Hot electrons effect in a #23 NTD Ge sample. J. Low Temp. Phys. 1998;110:1013.

[16] Grannan SM, Richards PL, Hase MK. Numerical optimization of bolometric infrared detectors including optical loading, amplifier noise, and electrical nonlinearities. Int. J. Infrared. Mill. Waves 1997;18:319.

[17] Hanany S. Private communication; measurements were done with A. T. Lee, B. Rabii, P. L. Richards and C. D. Winant of the MAXIMA team.

[18] Pobell F. Matter and Methods at Low Temperatures. Springer, 1992.

[19] Wang N, Wellstood FC, Saduolet B, et al. Electrical and thermal properties of neutron-transmutation-doped Ge at 20mK. Phys. Rev. B 1990;41:3761.

[20] Zhang J, Cui W, Juda M, et al. Non-ohmic effects in hopping conduction in doped silicon and germanium between 0.05 and 1 K. Phys. Rev. B 1998;57:4472.

[21] Wakui E, et al. In preparation, 2002.